Journal of Power Sources 204 (2012) 182–186

Contents lists available at SciVerse ScienceDirect

Journal of Power Sources

journal homepage: www.elsevier.com/locate/jpowsour

Short communication

Enhanced rate performance of two-phase carbon coated $LiFePO_4$/(C+G) using natural graphite as carbon source

Xuelin Yang[a,*], Fei Mou[a], Lulu Zhang[a], Gang Peng[a], Zhongxu Dai[a], Zhaoyin Wen[b,*]

[a] College of Mechanical and Material Engineering, Three Gorges University, 8 Da xue Road, Yichang 443002, PR China
[b] Shanghai Institute of Ceramics, Chinese Academy of Sciences, 1295 Ding xi Road, Shanghai 200050, PR China

ARTICLE INFO

Article history:
Received 8 September 2011
Received in revised form
10 December 2011
Accepted 14 December 2011
Available online 24 December 2011

Keywords:
Lithium iron phosphate
Natural graphite
Two-phase carbon
Electrochemical properties

ABSTRACT

The electrochemical performance of $LiFePO_4$/C samples synthesized by different carbon sources varies considerably, the structural difference of residual carbon in $LiFePO_4$/C accounts for the performance variation. Higher performance is associated with a larger ratio of graphitic carbon, which exhibits better electronic conductivity than amorphous carbon. To improve the electronic conductivity, we prepared $LiFePO_4$/(C+G) composites by a one-step solid-state method, in which natural graphite is used as reducing agent and conducting additives. The samples were characterized by X-ray diffraction (XRD), high-resolution transmission electron microscope (HRTEM), Raman microprobe spectroscope and other electrochemical methods. The results show that reversible capacity and rate performance of $LiFePO_4$ are improved considerably by the two-phase carbon coating. Therefore, $LiFePO_4$/(C+G) composites are a promising candidate for lithium ion batteries.

1. Introduction

Olivine $LiFePO_4$ is regarded as the one of the most promising alternative cathode materials for lithium ion batteries due to its advantages of high theoretic capacity (170 mAh g^{-1}), low cost, high safety and environmental friendliness [1–4]. However, $LiFePO_4$ could deliver its theoretical capacity only at a very low current density because of its poor electronic conductivity (10^{-9}–10^{-7} S cm^{-1}) and slow lithium ion diffusion [3–6]. Great efforts have been devoted to improving electrochemical performance of $LiFePO_4$, such as carbon coating [6,7], supervalent-cation doping [3,8,9] and nano-sized material designing [4,10]. Carbon coating is the most commonly used method for electrical conductivity improvement of $LiFePO_4$. Generally, there are two types of carbon sources, i.e. organic (e.g. glucose [11,12], sucrose [13], citric acid [14], PEG [15,16], etc.) and inorganic (e.g. AC-K5 [17], CMK-3 [18], CNTs [19], etc.). Among them, pyrolytic carbon from organic sources and conventional inorganic sources are commonly used; however, its amorphous feature impairs the reversible capacity and tap density of LFP [20]. Effects of graphitization degree of the incorporated carbon on cycling stability of $LiFePO_4$ has been proved in previous literatures [11,12], but it is hard to improve graphitization degree of pyrolytic carbon at the typical sintering temperature (<750 °C) of $LiFePO_4$. As a better conducting additive, high dispersed graphite or graphene [21] has been proved effective to improve high rate performance of $LiFePO_4$, but the graphite is inactive to reduce Fe^{3+}-containing component to form $LiFePO_4$ because of its structural stability. It is very essential to enhance the degree of an amorphous carbon with balanced ability to reduce Fe^{3+} and improve the tap density of the carbon coated $LiFePO_4$.

In this paper, natural graphite was first time applied as the reducing agent and conducting additive to prepare the two-phase carbon coated $LiFePO_4$/(C+G) cathode material. For this purpose, the graphite was miraculously activated and coated on $LiFePO_4$ by high-energy mechanical milling. XRD, TEM, Raman, cyclic voltammetry (CV) and charge/discharge tests were employed to investigate the samples.

2. Experimental

2.1. Sample synthesis

To prepare LFP/(C+G) cathode composite, Li_2CO_3, Fe_2O_3, $NH_4H_2PO_4$ (molar ratio of Li:Fe:P = 1.005:1:1) and natural graphite were used as starting materials. The graphite, activated by high-energy mechanical-milling, was ground with Li_2CO_3, Fe_2O_3 and $NH_4H_2PO_4$ for 6 h in alcohol to ensure homogeneous mixing. The mixture was dried at 60 °C overnight, sintered at 650 °C for 18 h in N_2 and cooled naturally.

* Corresponding authors. Tel.: +86 717 6392449; fax: +86 717 6397559.
E-mail addresses: xlyang@ctgu.edu.cn (X. Yang), zywen@mail.sic.ac.cn (Z. Wen).

0378-7753/$ – see front matter © 2011 Elsevier B.V. All rights reserved.
doi:10.1016/j.jpowsour.2011.12.032

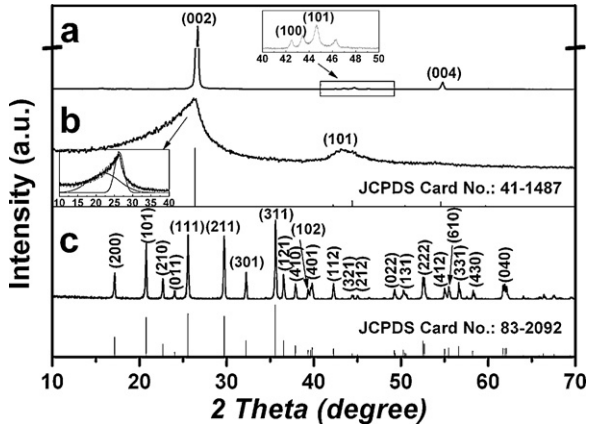

Fig. 1. X-ray diffraction patterns of (a) NG, (b) HEMM-G, and (c) LFP/ (C+G).

2.2. Sample analysis

The phase and crystalline structure of LFP/(C+G) composite were studied by X-ray diffraction (XRD, Rigaku RINT-2000) with Cu-kα radiation (λ = 1.5406 Å). The morphology was observed with field-emission scanning electron microscope (FE-SEM, JSM7500F, JEOL), and the structure was characterized by transmission electron microscopy (TEM, JEM-2010). Carbon coating on the as-prepared LFP/(C+G) particles was estimated by Raman spectra (VERTEX 70, Bruker) and carbon content was determined by carbon–sulfur analyzer (CS600, LECO, US). The tap density of the LFP/(C+G) sample was measured by the tap density measurement instrument (JZ-1, China).

2.3. Electrochemical measurement

The working electrodes were prepared by mixing active material LFP/(C+G) with PVDF binder and acetylene black in a weight ratio of 75:15:10 in *N*-methyl pyrrolidinone solvent. The resulting slurry was cast on an aluminum foil using an automatic film-coating equipment to control film thickness. The film was punched into disc (Φ 14 mm) and pressed (6 MPa). After drying at 120 °C for 8 h in vacuum, the disc was transferred into an argon-filled glove box (<1 ppm H_2O, <1 ppm O_2), the loading of LFP/C on the electrode is about 1.27 mg cm^{-2}. 2025 coin cells were assembled using Celgard 2400 as separator, lithium foil as counter and reference electrode, and 1 M $LiPF_6$/(EC + DMC, 1:1 in mass) as electrolyte. The cells were tested at various rates in the voltage range of 2.5 and 4.2 V (vs. Li^+/Li) at room temperature on a cell testing instrument (LAND CT2001A, China). Cyclic voltammetry (CV) measurements were performed on an electrochemical working station (PARSTAT 2273, Princeton

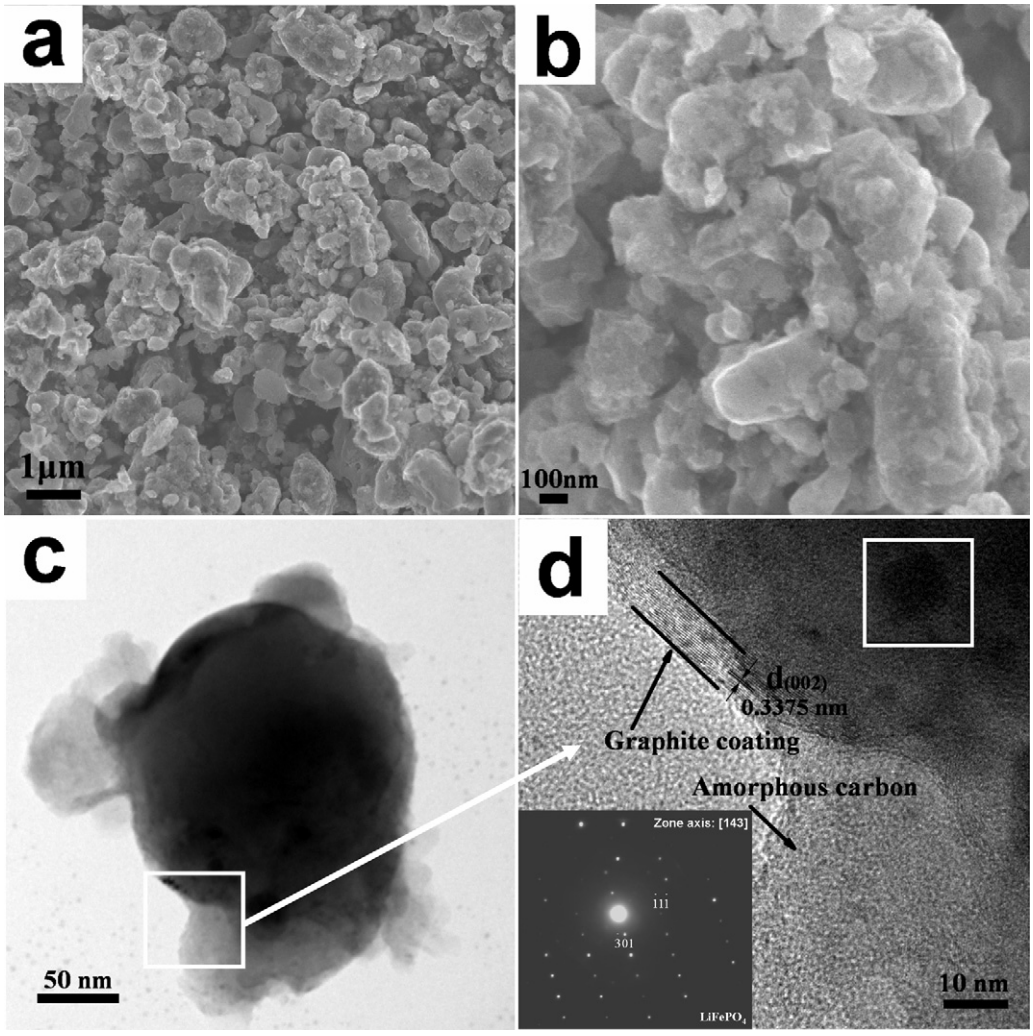

Fig. 2. (a and b) SEM and (c and d) TEM images of the LFP/(C+G) composite.

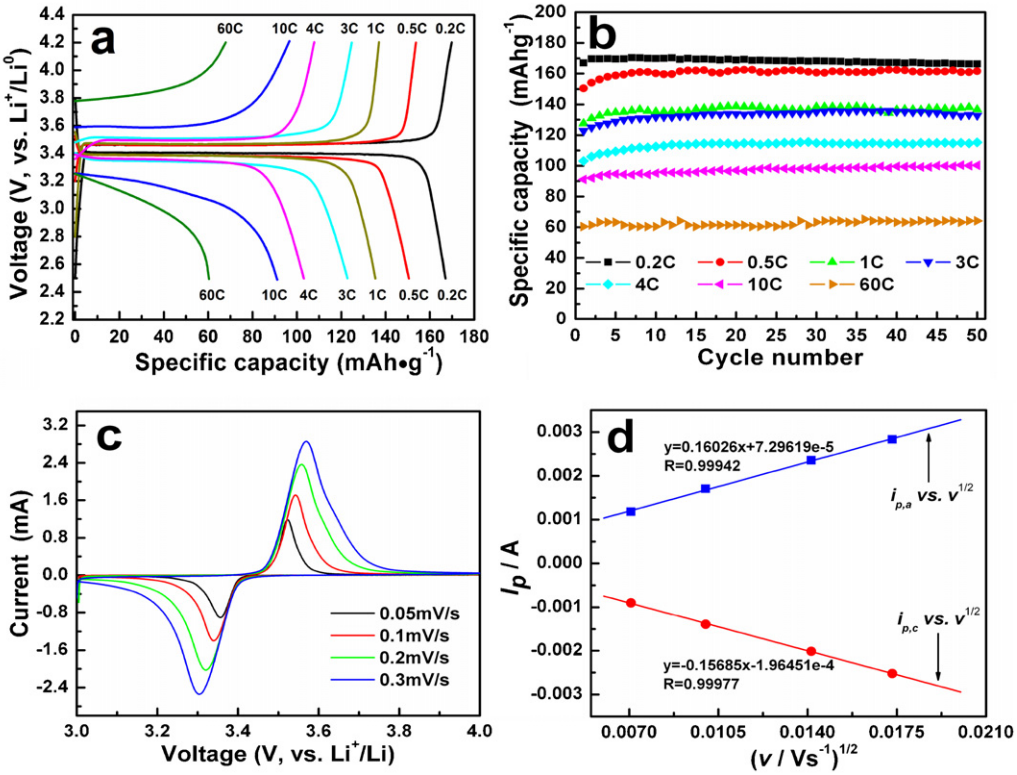

Fig. 3. (a) The initial charge/discharge voltage curves, (b) the cyclic performance for LFP/(C+G) electrodes at different *C*-rates, (c) CV curves of LFP/(C+G) electrodes at scan rates of 0.05, 0.1, 0.2, 0.3 mV s^{-1}, respectively, between 3.0 V and 4.0 V (vs. Li/Li^+), and (d) relationship between $i_{p,a}/i_{p,c}$ and $\nu^{1/2}$.

Applied Research, USA) at a scanning rate of 0.05 mV s^{-1} within a voltage range of 3.0–4.0 V.

3. Results and discussion

Fig. 1 shows the XRD patterns of natural graphite (NG), activated graphite by high-energy mechanical-milling treatment (HEMM-G) and LFP/(C+G). As seen in Fig. 1, the activated graphite shows a clear asymmetric peak at about 26° which can be deconvoluted into two peaks: one (at ~23°) is for amorphous carbon and the other (at ~26°) for graphitic carbon. The peak (at ~26°) broadening may be related to the decrease in crystal size of graphite after mechanical activation. The crystal sizes of natural graphite and activated graphite estimated by *Scherrer's* equation are 33 nm and 1 nm, respectively, calculated from the (0 0 2) plane of the two samples. Apparently, the size of activated graphite decreases after high-energy mechanical-milling. In addition, for the activated graphite, the second peak (~42°) corresponding to (1 0 1) plane of graphite (JCPDS No. 41-1487), is observed. However, this peak is more clear and broader than that for natural graphite, due to the overlap with (1 1 1) plane of Fe_3C (JCPDS No. 89-2005), which is formed during the high-energy mechanical milling. However, Fe_3C impurity disappears in the XRD pattern for LFP/(C+G) sample because of decomposition and consumption for LFP/C formation during the high-temperature sintering process. The diffraction peaks for LFP/(C+G) composite are well indexed to orthorhombic $LiFePO_4$ (JCPDS No. 83-2092) with space group of *Pnma*, the cell parameters are as follows: $a = 10.336$ Å, $b = 6.013$ Å, $c = 4.695$ Å, $V = 291.85$ $Å^3$, which are very close to the ideally crystallized $LiFePO_4$ ($a = 10.334$ Å, $b = 6.010$ Å, $c = 4.693$ Å, $V = 291.47$ $Å^3$) and the previous reports [22,23]. Average crystal size of LFP/(C+G) sample is about 65 nm, calculated from the (1 0 1), (1 1 1), (2 1 1) and (3 1 1) planes of orthorhombic $LiFePO_4$. Furthermore, other impurity phases, such as α-Fe_2O_3, Fe_2P [24,25], disappear in our case, indicating excellent reduction ability of the activated carbon for Fe^{3+} to Fe^{2+}.

Fig. 2 shows the SEM and TEM images of LFP/(C+G) samples. As shown in Fig. 2a and b, LFP/(C+G) particles present irregular shapes with a wide size-distribution ranging from ~100 nm to 1.5 μm, and most LFP/(C+G) particles are micron-sized. To analyze the structure of the coating layer and the substrate, a nano-particle was selected to be observed (Fig. 2c and d). It is found that graphite and amorphous carbon are wrapping and/or connecting the as-prepared LFP/(C+G) particles. The electron diffraction patterns in Fig. 2d clearly indicated that the coating consisted of two kinds of carbon phase, i.e. graphite and amorphous carbon (carbon content in the composite is 2.12%). The thinner coating (<10 nm) on the surface of the LFP particles displays clear crystal planes with a d-spacing of 0.3375 nm corresponding to the (0 0 2) plane of hexagonal graphite. The thicker coating is apparently characterized as amorphous carbon. The selected area electron diffraction (SAED) pattern in the insert of Fig. 2d indicates the substrate as orthorhombic LFP clearly.

The tap density of LFP/(C+G) sample is 1.413 g cm^{-3}, which is higher than that of previously reported data [20,26,27]. The high tap density attributes to the suitable gradation of nano-sized and micron-sized particles (Fig. 2a and b), i.e. nano-sized particles can efficiently fill up the gaps between the micron-sized particles. High tap density provides a possibility for the as-prepared LFP/(C+G) to exhibit excellent high-rate electrochemical performance without sacrificing the volumetric energy density.

The charge/discharge characteristics of the first cycle and the cyclic performance of LFP/(C+G) electrodes at different *C*-rate are shown in Fig. 3a and b, respectively. As seen, the capacity drops

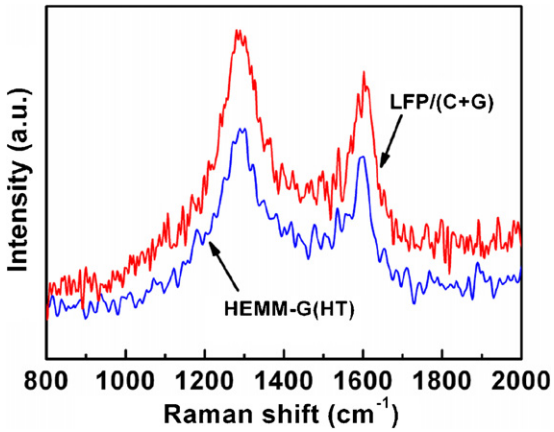

Fig. 4. Raman spectra of LFP/(C+G) and HEMM-G (HT).

with increase of *C*-rate, indicating that the capacity loss is restricted by lithium-ion diffusion. The LFP/(C+G) electrode shows a charge capacity as high as 167.0 mAh g^{-1} at 0.2*C*, which is equivalent to 98% of the theoretical capacity. Furthermore, LFP/(C+G) exhibits 135.4 mAh g^{-1}, 103.1 mAh g^{-1}, 91.1 mAh g^{-1} and 60.4 mAh g^{-1} at 1*C*, 4*C*, 10*C* and 60*C*, respectively, which are apparently higher than those of LFP/C samples coated with only amorphous carbon [28]. Remarkably, no detectable decline in capacity was observed after over 100 cycles even at 60*C* for the LFP/(C+G) electrode. The high capacity retention ability of the LFP/(C+G) composite at different *C*-rate indicates that the two-phase coating consisting of graphite and amorphous carbon can form a barrier to electrolyte and alleviate the iron dissolution during cycling, resulting from the flake structure of graphite coating, and improves the reversibility of Li^+ extraction/insertion [29]. CV curves of the LFP/(C+G) electrodes are shown in Fig. 3c, and the signals were monitored at gradually increased scan rates from 0.05 to 0.3 mV s^{-1}. As found, the lower the scan rate, the smaller the difference between the reduction and the oxidation potentials, demonstrating the less polarization under a lower scan rate. The lithium ion diffusion coefficient can be evaluated from a relationship between anodic/cathodic peak currents ($i_{p,a}/i_{p,c}$) and the square root of scan rates ($\nu^{1/2}$) according to the *Randles-Sevcik* equation [30]. As shown in Fig. 3d, the anodic and cathodic diffusion coefficients of lithium ion are calculated to be 2.54×10^{-9} and 2.43×10^{-9} cm^2 s^{-1}, respectively. Obviously, the anodic diffusion coefficient of lithium ion is very close to the cathodic diffusion coefficient of lithium ion, which demonstrates a good reversibility. This result also reveals that the two-phase carbon coating facilitates the kinetic process of the electrochemical reactions.

Raman spectroscopy in the field of $LiFePO_4$-based cathode materials is a very convenient diagnostic tool to evaluate the quality of the carbon coating on $LiFePO_4$ powders and films [31,32]. Fig. 4 shows the Raman spectra of the LFP/(C+G) and HEMM-G heat-treated at 650 °C for 18 h in N_2 (labeled as HEMM-G(HT)) samples. Two intense broad bands at 1305 and 1590 cm^{-1} are assigned to the D (sp^3-type) and G (sp^2-type) bands of the residual carbon in the samples, respectively. The variation of the width and intensity of the D and G bands is related to the growth and size of different carbon phases, the presence of functional groups and impurities [33]. As shown in XRD patterns, part of graphite has been converted to amorphous carbon after high-energy mechanical milling. During high-temperature sintering process, amorphous carbon with disordered feature is less thermodynamic stable than graphite, thus it is more easily consumed to reduce Fe^{3+} to Fe^{2+}. As shown in Fig. 4, there is no obvious difference in the positions of D and G bands between LFP/(C+G) and HEMM-G(HT), but the integrated D/G intensity ratio for LFP/(C+G) (1.679) is lower than that for HEMM-G(HT) (2.136), indicative of the consumption of a part of amorphous carbon for reducing Fe^{3+} to Fe^{2+}. Therefore, it is reasonable to believe that the amorphous carbon is determinant for reduction, while the residual graphite plays a dominant role in improving the electronic conductivity, which results in an enhanced electrochemical performance of the LFP/(C+G) composite.

4. Conclusions

A novel two-phase carbon coated LFP/(C+G) cathode material has been prepared using natural graphite as the carbon source. The as-prepared LFP/(C+G) exhibits an initial charge capacity as high as 167.0 mAh g^{-1} with a coulombic efficiency of 98.4% at 0.2*C*, and excellent rate capacity of 91.1 mAh g^{-1} and 60.4 mAh g^{-1} even at 10*C* and 60*C*, respectively, and favorable electrochemical cyclability at different *C*-rate. These results suggest that the application of natural graphite in preparing LFP would be an economical, effective way and promising for lithium ion batteries, and is suitable for the large-scale production of batteries such as those used in EVs or HEVs.

Acknowledgments

This work was financially supported by Natural Science Foundation of China (NSFC, 50972075), key projects of Chinese Ministry of Education (D209083) and Excellent Youth Foundation of Hubei Scientific Committee (2011CDA093). Moreover, the authors are grateful to Dr. Jianlin Li at Three Gorges University for his kind support to our research.

References

[1] A.K. Padhi, K.S. Nanjundaswamy, J.B. Goodenough, J. Electrochem. Soc. 144 (1997) 1188–1194.
[2] L.X. Yuan, Z.H. Wang, W.X. Zhang, X.L. Hu, J.T. Chen, Y.H. Huang, J.B. Goodenough, Energy Environ. Sci. 4 (2011) 269–284.
[3] S.Y. Chung, J.T. Bloking, Y.M. Chiang, Nat. Mater. 1 (2002) 123–128.
[4] P. Gibot, M. Casas-Cabanas, L. Laffont, S. Levasseur, P. Carlach, S.P. Hamelet, J.M. Tarascon, C. Masquelier, Nat. Mater. 7 (2008) 741–747.
[5] C. Delacourt, L. Laffont, R. Bouchet, C. Wurm, J.-B. Leriche, M. Morcrette, J.-M. Tarascon, C. Masquelier, J. Electrochem. Soc. 152 (2005) A913–A921.
[6] Y.H. Huang, J.B. Goodenough, Chem. Mater. 20 (2008) 7237–7241.
[7] G.X. Wang, L. Yang, S.L. Bewlay, Y. Chen, H.K. Liu, J.H. Ahn, J. Power Sources 146 (2005) 521–524.
[8] P.S. Herle, B. Ellis, N. Coombs, L.F. Nazar, Nat. Mater. 3 (2004) 147–152.
[9] L.-L. Zhang, G. Liang, A. Ignatov, M.C. Croft, X.-Q. Xiong, I.-M. Hung, Y.-H. Huang, X.-L. Hu, W.-X. Zhang, Y.-L. Peng, J. Phys. Chem. C 115 (2011) 13520.
[10] M. Gaberscek, R. Dominko, J. Jamnik, Electrochem. Commun. 9 (2007) 2778–2783.
[11] X.K. Zhi, G.C. Liang, L. Wang, X.Q. Ou, L.M. Gao, X.F. Jie, J. Alloys Compd. 503 (2010) 370–374.
[12] X.H. Liu, Z.W. Zhao, Powder Technol. 197 (2010) 309–313.
[13] Y. Kadoma, J.-M. Kim, K. Abiko, K. Ohtsuki, K. Ui, N. Kumagai, Electrochim. Acta 55 (2010) 1034–1041.
[14] V. Palomares, A. Goñi, I. Gil de Muro, I. de Meatza, M. Bengoechea, I. Cantero, T. Rojo, J. Electrochem. Soc. 156 (2009) A817–A821.
[15] Y.Y. Liu, C.B. Cao, J. Li, Electrochim. Acta 55 (2010) 3921–3926.
[16] Z.H. Xu, L. Xu, Q.Y. Lai, X.Y. Ji, Mater. Res. Bull. 42 (2007) 883–891.
[17] M. Yang, Q.M. Gao, J. Alloys Compd. 509 (2011) 3690–3698.
[18] G.X. Wang, H. Liu, J. Liu, S.Z. Qiao, G. Max Lu, P. Munro, H. Ahn, Adv. Mater. 22 (2010) 4944–4948.
[19] Y.K. Zhou, J. Wang, Y.Y. Hu, R. O'Hayre, Z.P. Shao, Chem. Commun. 46 (2010) 7151–7153.
[20] Z. Chen, J.R. Dahn, J. Electrochem. Soc. 149 (2002) A1184–A1189.
[21] Y. Ding, Y. Jiang, F. Xu, J. Yin, H. Ren, Q. Zhuo, Z. Long, P. Zhang, Electrochem. Commun. 12 (2010) 10–13.
[22] J. Liu, T.E. Conry, X.Y. Song, M.M. Doeff, T.J. Richardson, Energy Environ. Sci. 4 (2011) 885–888.
[23] Y.H. Huang, H.B. Ren, S.Y. Yin, Y.H. Wang, Z.H. Peng, Y.H. Zhou, J. Power Sources 195 (2010) 610–613.
[24] M.E. Zhong, Z.T. Zhou, Mater. Chem. Phys. 119 (2010) 428–431.
[25] G.T.-K. Fey, K.-P. Huang, H.-M. Kao, W.-H. Li, J. Power Sources 196 (2011) 2810–2818.

[26] X.M. Lou, Y.X. Zhang, J. Mater. Chem. 21 (2011) 4156–4160.
[27] S.W. Oh, H.J. Bang, S.-T. Myung, Y.C. Bae, S.-M. Lee, Y.-K. Sun, J. Electrochem. Soc. 155 (2008) A414–A420.
[28] H. Liu, P. Zhang, G.C. Li, Q. Wu, Y.P. Wu, J. Solid State Electrochem. 12 (2008) 1011–1015.
[29] S.W. Oh, S.-T. Myung, S.-M. Oh, K.H. Oh, K. Amine, B. Scrosati, Y.-K. Sun, Adv. Mater. 22 (2010) 4842–4845.
[30] J.R. Dahn, J. Jiang, L.M. Moshurchak, M.D. Fleischauer, C. Buhrmester, L.J. Krause, J. Electrochem. Soc. 152 (2005) A1283–A1289.
[31] M.M. Doeff, Y.Q. Hu, F. McLarnon, R. Kostecki, Electrochem. Solid-State Lett. 6 (2003) A207.
[32] R. Baddour-Hadjean, J.-P. Pereira-Ramos, Chem. Rev. 110 (2010) 1278–1319.
[33] J.D. Wilcox, M.M. Doeff, M. Marcinek, J. Kostecki, J. Electrochem. Soc. 154 (2007) A389–A395.